

## Ideal Cleavage Process in Weakly Stable Systems

Václav Paidar

Institute of Physics AS CR vvi, Na Slovance 2, 182 21 Praha 8, Czech Republic

paidar@fzu.cz

**Keywords:** ideal strength,  $\gamma$ -surfaces, localized cleavage, homogeneous shear

**Abstract.** The ideal cleavage strength is calculated for the many-body potentials describing weakly stable cubic structures. The cleavage strength is compared with the ideal shear strength that is discussed from the point of view of the energetically lowest shear path to break the crystal. The exponential semiempirical interatomic potentials have been chosen to reflect the behaviour of materials undergoing displacive martensitic phase transformations.

### Introduction

Ideal strength is a fundamental intrinsic material parameter characterizing the behaviour far from the equilibrium. Together with the elastic constants the ideal strength provides the basic input to the models of mechanical properties [1]. The breaking and reformation of atomic bonds controls the mobility of crystal defects and thus also the mechanical behaviour of materials. This quantity obviously reflects underlying chemical bonding and related structural stability of studied systems.

Not only electrical and magnetic properties of materials are determined by events occurring on the subatomic scale. With the ultimate aim to understand displacive martensitic phase transformations the interatomic forces suitable for description of weakly stable systems are investigated in this paper. So far mostly the geometrical models without sufficient account of atomistic nature of transformation processes are applied for descriptions of diffusionless transformations [2].

First, the calculations of the interaction between two half-crystals leading to the ideal cleavage strength will be reported. Then the concept of ideal shear strength will be discussed on the basis of G-surface for homogeneous shear deformation – superposition of generalized stacking faults on all parallel atomic planes. The notation G-surface is used here to distinguish the  $\gamma$ -surface for two-dimensional objects as free surfaces or stacking faults from the three-dimensional objects as homogeneously sheared crystals.

Since the lattice instability is essential for displacive phase transitions, such many-body interatomic potentials were chosen to mimic transitions between bcc, hcp and fcc structures. The potentials were fitted to the fcc crystal characterized by the cohesive energy and lattice parameter and the bonding attractive forces were varied to get bcc or hcp lattices more stable.

### Interatomic Many-Body Potentials

Finnis-Sinclair type many-body potentials have been chosen for our calculation. The exponential form of the potentials [3] with only five parameters is used. The total cohesive energy is expressed as a sum over all atoms in the system

$$E = - \sum_i (E_b^i + E_r^i), \quad (1)$$

and it is composed of the bonding contributions based on the d-band density of electron states

$$E_b^i = - \left\{ \sum_j \xi^2 \exp \left[ -2q \left( \frac{r_{ij}}{r_0} - 1 \right) \right] \right\}^{1/2} \quad (2)$$

and contributions of repulsive forces represented by the pair-wise potential of Born-Mayer type

$$E_r^i = \sum_j A \exp \left[ -p \left( \frac{r_{ij}}{r_0} - 1 \right) \right]. \quad (3)$$

The energy is then given by four adjustable parameters  $\xi$ ,  $A$ ,  $p$  and  $q$ . Two parameters,  $p$  and  $q$ , are dimensionless and two,  $A$  and  $\xi$ , are in units of energy.  $r_{ij}$  is the interatomic distance between the atoms  $i$  and  $j$ .

Two potential parameters were fitted to the cohesive energy and lattice parameter to obtain reasonable energy and length scaling. The other two parameters  $p$  and  $q$  in exponents were changed freely to reduce the structural stability. Fitting was performed to the cohesive energy of 2.95 eV and the lattice parameter of 0.409 nm (corresponding to silver) for all chosen values of  $p$  and  $q$ . The fifth parameter  $r_0$  is equal to the first neighbour separation in the fcc lattice.

Both the bonding,  $E_b^i$ , and repulsive,  $E_r^i$ , energy contributions for an  $i$ -atom are cut off at the distance corresponding to the 4<sup>th</sup> neighbours of the fcc lattice. Between the 3<sup>rd</sup> and 4<sup>th</sup> neighbours, the exponential expressions for  $E_b^i$  and  $E_r^i$  (eqs. (2) and (3)) are replaced by fifth order polynomials. The polynomial coefficients are fitted to obtain continuity of the values and first and second derivatives at the point of line-up at the distance of the 3<sup>rd</sup> neighbours and truncation to zero at the cut-off distance of the 4<sup>th</sup> neighbours.

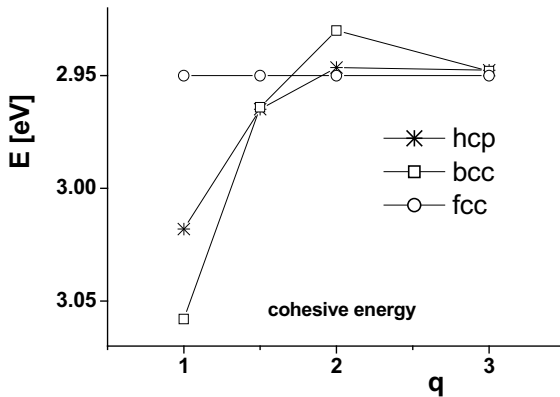


Fig. 1. Cohesive energy for fcc, bcc and hcp structures as a function of the parameter  $q$ .

It was found [4] that the bcc lattice is favoured for small values of  $q$  and the hcp structure is the most stable in between the regions of bcc and fcc stability. Since the commonly used values of  $p$  and  $q$  are between 9-11 and 2-4, respectively, (see e.g. [5]) the repulsive pair-wise part was fixed at  $p=9$  and  $q$  varies between 1 and 2. It means that only the bonding part is altered while the repulsive part is kept constant. The potentials will be denoted by  $q$  and its value, e.g.  $q1$ .

The dependence of the cohesive energies for fcc, bcc and hcp structures on the parameter  $q$  is shown in Fig. 1. The bcc structure is the most stable for  $q=1$ , while for  $q=1.5$  the energies of bcc

and hcp are about the same and the bcc structure is less stable in comparison with the fcc and hcp at  $q=2$ .

The many-body potentials were systematically applied in the literature to study the external free surfaces (see for instance [6,7]). The free surfaces are a limit of ideal cleavage process when the two half-crystals are gradually separated on a chosen atomic plane starting from the perfect crystal. The results of such calculations are reported in the next section.

### Ideal Cleavage Strength

The energies were calculated for the crystals with the equilibrium interplanar spacing for all atomic planes with the exception of the two planes at the block centre. Their separation was gradually increased from the equilibrium value to such values when the total energy of the block remained unchanged. The calculations were performed for four atomic planes, the planes with the largest atomic densities, i.e. (111) in fcc and (101) in bcc crystals, and for the (001) surfaces in both cubic lattices.

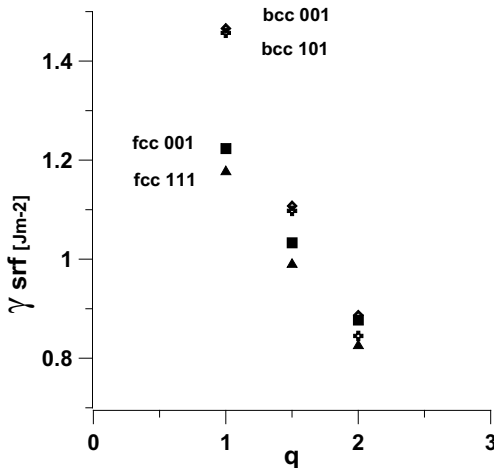


Fig. 2. Free surface energies for four surface planes as functions of parameter  $q$ . The (001) surfaces are denoted by squares and diamonds for fcc and bcc lattices, respectively, the densest surfaces by triangles and crosses.

Bonding energies for the bcc structures and  $q_1$  potential are larger than for the fcc structures (see Fig. 1) and thus also the free surface energies are larger. The lowest free surface energy was obtained for the close-packed (111) fcc surface for all the tested potentials (see Fig. 2). The difference between the bcc and fcc surface energies for the densest surface planes is large for  $q_1$ , however, for the  $q_2$  potential the (101) bcc surface energy is close to the (111) fcc surface energy in spite of the fact that bcc and fcc cohesive energies are different (see Fig. 1).

The experimental values of the free surface energy are estimated in [8], for silver it is about  $1.3 \text{ Jm}^{-2}$  at low temperatures. This value is comparable with our results for  $q_1$  potential while for  $q_2$  the surface energies are about 30% lower. Using Embedded Atom Method (EAM) even lower values were obtained for Ag [6]. The agreement with experiment was improved by modified EAM potential [7].

The energies of two rigid crystal parts separated by the increasing gap of vacuum are depicted in Fig. 3 and 4. The energy of the perfect crystals (bcc or fcc) is chosen as the zero level for ideal

cleavage process. The excess energies with respect to the perfect crystals that are expressed in units of energy density per unit area of separation planes are steadily growing with humps corresponding to the separations where the atomic plane interaction is passing through the potential cut-off distances. The constant level indicates that two crystal halves are not interacting when they are separated more than potential cut-off radius. Since the equilibrium atomic plane separation is the largest for the densest planes, the crystal halves interaction is lost for the smallest gap width in equilibrium-atomic-plane-spacing units.

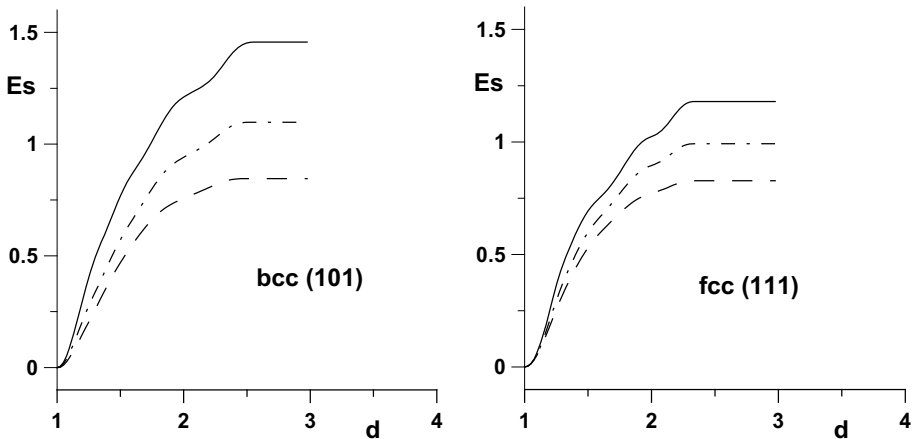


Fig. 3. Energy of two crystal blocks separated to the distance  $d$  for the (101) bcc and (111) fcc atomic planes. The energies  $E_s$  are expressed in  $\text{Jm}^{-2}$  and the separations  $d$  in the units of the equilibrium atomic plane spacing. Full line q1 potential, dot-dashed line q1.5 potential, dashed line q2 potential.

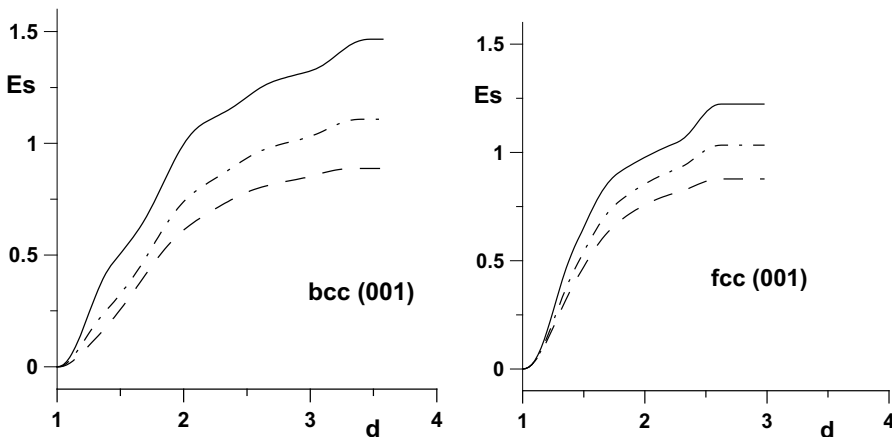


Fig. 4. Energy of two crystal blocks separated to the distance  $d$  for the (001) bcc and (001) fcc atomic planes. The same notation as in Fig. 3.

The derivatives  $dEs$  of the curves presented in Fig. 3 and 4 with respect to the half-crystal separation give the ideal cleavage forces for chosen atomic planes. Those are shown in Fig. 5 and 6 expressed in  $Jm^{-3}$  SI units. The shape of these curves is similar to those published in [9] for Cu and the many-body potential from [10].

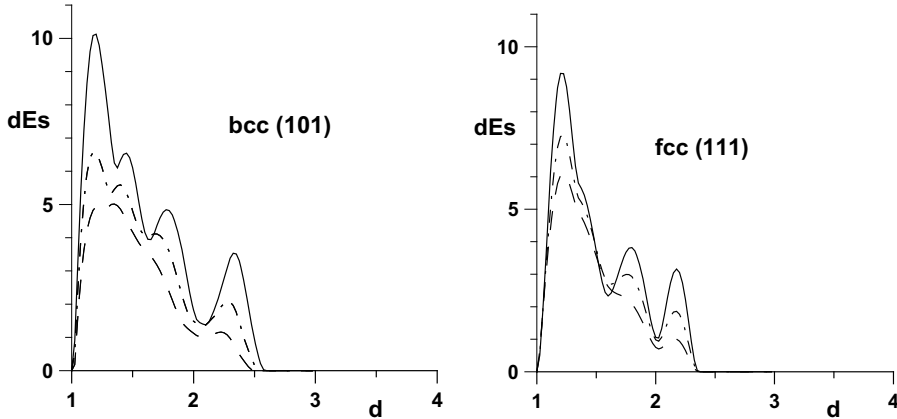


Fig. 5. Ideal cleavage force, expressed in  $Jm^{-3}$ , acting between two crystal blocks separated to the distance  $d$  for the (101) bcc and (111) fcc atomic planes. The same notation as in Fig. 3.

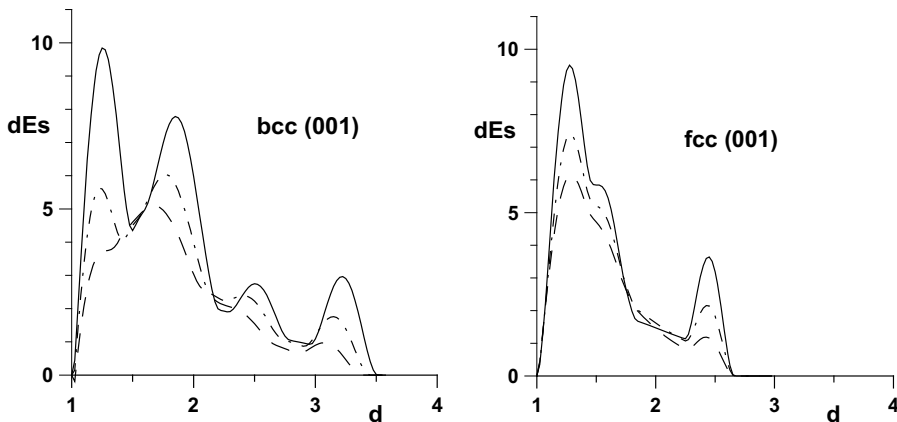


Fig. 6. Ideal cleavage force, expressed in  $Jm^{-3}$ , acting between two crystal blocks separated to the distance  $d$  for the (001) bcc and (001) fcc atomic planes. The same notation as in Fig. 3.

The ideal cleavage forces are compared with the elastic moduli [11] in the respective loading directions in Table 1. The cleavage force in the [001] direction is normalized by  $C001=c_{11}$ , in the [101] direction by  $C101=(c_{11}+c_{12}+2c_{44})/2$  and in the [111] direction by  $C111=(c_{11}+2c_{12}+4c_{44})/3$ . The ideal cleavage forces are expressed in % of the respective elastic moduli. While the cleavage force on both bcc planes is about of the same relative magnitude it is significantly decreasing with growing  $q$  for both fcc cleavage planes.

The magnitudes of all calculated ideal cleavage forces are compared in Fig. 7. For  $q_1$  the lowest value is obtained for the (111) fcc cleavage plane while for  $q_2$  it is for the (101) bcc cleavage plane. The cleavage forces are decreasing with growing  $q$  for all studied cleavage planes.

Table 1. Ideal cleavage forces and elastic moduli for straining in the direction perpendicular to the cleavage plane.

bcc	q	1	1.5	2	fcc	q	1	1.5	2
C001 GPa		208	163	102	C001 GPa		47	61	74
dEs bcc (100) %C001		4.7	3.7	5.0	dEs fcc (100) %C001		20.1	12.1	8.3
C101 GPa		228	184	133	C111 GPa		66	85	103
dEs bcc (101) %C101		4.4	3.6	3.7	dEs fcc (111) %C111		13.8	8.6	5.9

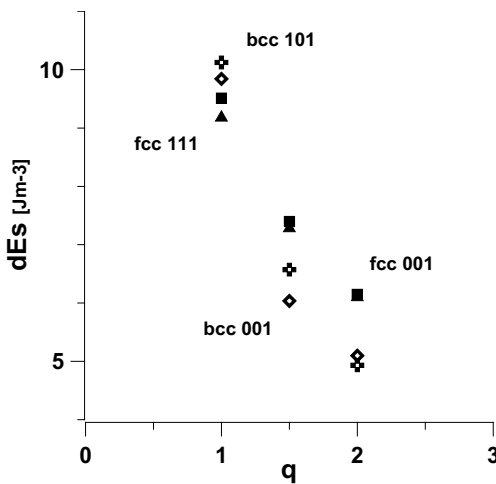


Fig. 7. Ideal cleavage force for four surface planes as functions of parameter  $q$ . The same surfaces are considered as in Fig. 2.

### Ideal Shear Strength

Let us discuss here the ideal shear strength on the (101) plane in bcc lattice for  $q_{1.5}$  potential. Similarly to the calculations of  $\gamma$ -surfaces for generalized stacking faults, i.e. planar defects, where the upper crystal half is shifted with respect to the lower crystal half [12], we can calculate generalized shear energies, that have volume character, for the displacements repeated on every atomic plane. The displacement vector is any vector on the selected plane and the resulting G-surface for homogeneously sheared three-dimensional crystal has periodicity of the atomic plane on which the displacements are realized as in the case of  $\gamma$ -surface for two-dimensional crystal defects. Such a G-surface is shown in Fig. 8.

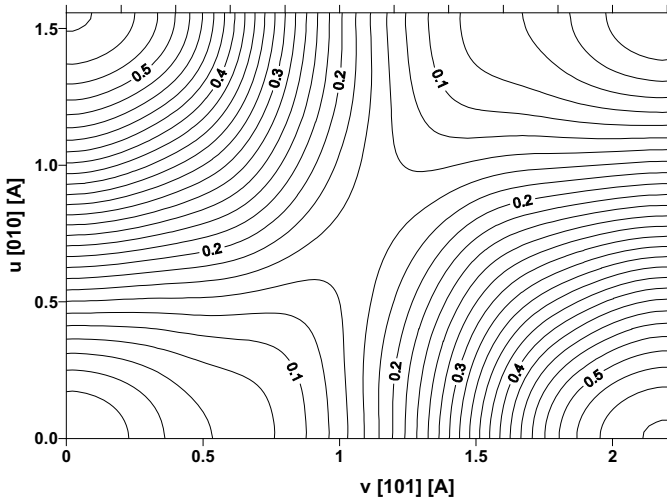


Fig. 8. G-surface for generalized shear deformation on the (101) bcc plane for q1.5 potential. The displacements up to  $\frac{1}{2}[010]$  and  $\frac{1}{2}[101]$  are given in Angstrom =  $10^{-10}$  m, the energies in eV =  $16.021 \cdot 10^{-20}$  J.

The ideal shear strength is usually calculated along the direction of the Burgers vector, i.e.  $\frac{1}{2}[111]$  [13], but it is seen in Fig. 8 that the valley of the steepest descent from the saddle point is along the [121] direction. This is why the ideal shear strength as the derivative of the G-surface was calculated not only along the diagonal [111] but also along [121] see Fig. 9.

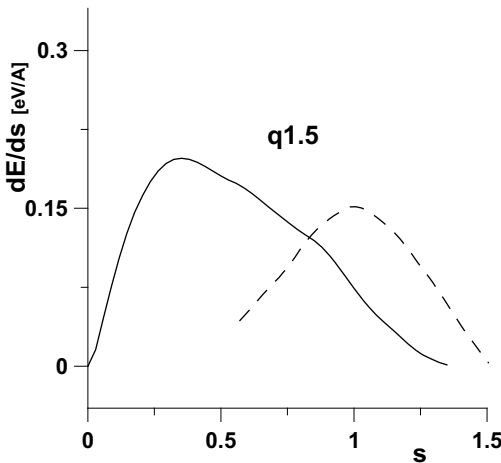


Fig. 9. Ideal shear strength along [111] - full line and along [121] – dashed line on the (101) bcc plane for q1.5 potential.

It is shown in Fig. 9 that the shear force necessary to overcome the saddle point on the G-surface is 23% lower along the [121] direction than along [111]. While it is 9.58% of the respective shear modulus on (101) in [111] it is only 7.35% along the [121] direction.

## Summary

The ideal cleavage strength on the (101) and (001) atomic planes does not reflect the bcc lattice instability, it remains on the same relative level with respect to the respective elastic moduli. The ideal shear strength is found to be significantly lower along the [121] direction than along [111] that is usually considered in the literature as the shear direction.

**Acknowledgements** The support by the COST program P19 OC149 is gratefully appreciated.

## References

- [1] J. Li, A.H.W. Ngan, P. Gumbsch, *Acta Mater.* 51 (2003) 5711.
- [2] R.C. Pond, S. Celotto, J.P. Hirth, *Acta Mater.* 51 (2003) 5385.
- [3] V. Rosato, M. Guillopé, B. Legrand, *Phil. Mag. A* 59 (1989) 321.
- [4] A. Ostapovets, V. Paidar, *Mater. Sci. Forum* 567-8 (2007) 69.
- [5] O. Hardouin Duparc, A. Larere, B. Lezzar, O. Khalfallah, V. Paidar, *J. Mater. Sci.* 40 (2005) 3169.
- [6] S.M. Foiles, M.I. Baskes, M.S. Daw, *Phys. Rev. B* 33 (1986) 7983.
- [7] J.M. Zhang, Y. Shu, K.W. Xu, *Solid State Comm.* 137 (2006) 441.
- [8] W.R. Tyson, W.A. Miller, *Surf. Sci.* 62 (1977) 267.
- [9] Y.N. Osetsky, D.J. Bacon, C.C. Matthai, N.H. March, *J. Phys. Chem. Solids* 61 (2000) 2055.
- [10] G.J. Ackland, G. Tichy, V. Vitek, M.W. Finnis, *Phil. Mag. A* 56 (1987) 735.
- [11] A. Ostapovets, V. Paidar, *Metallic Mater.* (2008) to be published.
- [12] V. Paidar, V. Vitek, in: *Intermetallic Compounds, Progress*, Vol. 3, J.H. Westbrook, R.L. Fleischer (eds.), John Wiley, Chichester, 2002, p. 437.
- [13] S. Ogata, J. Li, N. Hirotsaki, Y. Shibutani, S. Yip, *Phys. Rev. B* 70 (2004) 104104.